

Paper presented at the Ultrasonics International '99 and 1999 World Congress on Ultrasonics, Technical University of Denmark, Denmark:

Simulation of RF data with tissue motion for optimizing stationary echo canceling filters

Malene Schlaikjer¹, Søren Torp-Pedersen² and Jørgen Arendt Jensen²

¹Center for Fast Ultrasound Imaging,
Department of Information Technology, Build. 344,
Technical University of Denmark,
DK-2800 Lyngby, Denmark

²Department of Radiology
Gentofte University Hospital
Niels Andersensvej 65
DK-2900 Hellerup, Denmark

To be published in Ultrasonics, February 2000.

Simulation of RF data with tissue motion for optimizing stationary echo canceling filters

M. Schlaikjer¹, S. Torp-Pedersen², and J.A. Jensen¹

¹Department of Information Technology, Build. 344,
Technical University of Denmark, DK-2800 Lyngby, Denmark

²Department of Radiology, Gentofte University Hospital,
Niels Andersensvej 65, DK-2900 Hellerup, Denmark

Abstract

Blood velocity estimation is complicated by the strong echoes received from tissue surrounding the vessel under investigation. Proper blood velocity estimation necessitates use of a filter for separation of the different signal components. Development of these filters and new estimators requires RF-data, where the tissue component is known. *In-vivo* RF-data does not have this property. Instead simulated data incorporating all relevant features of the measurement situation can be employed. One feature is the motion in the surrounding tissue induced by pulsation, heart beat, and breathing. This study have developed models for the motions and incorporated them into the RF simulation program Field II, thereby obtaining realistic simulated data. The nature of pulsation is discussed, and a relation between the pressure in the carotid artery and the experienced vessel wall motion is derived.

1 Introduction

Ultrasound for cardiovascular imaging is widely used today for diagnostic purposes. From recorded RF-signals estimates of the velocity distribution of the blood flow can be computed, which can reveal cardiovascular diseases such as occlusions. Use of simulated RF-data is desirable, when developing new blood velocity estimators, stationary echo cancelling filters, and other filters for processing recorded RF-signals, since they are well defined. *In-vivo* RF-signals do not have this property, since the signal components from the surrounding tissue and the blood are not easily distinguishable, and the accurate extend of the vessel is unknown.

To obtain realistic simulated RF-data all relevant features of the measurement situation must be incorporated. One feature is the motion in the tissue surrounding the vessel under investigation induced by breathing, heart beat, and pulsation of arterial vessel walls. The motion is a result of a change in position of one or more organs (lung and heart), and vessel walls, whereby motion is induced upon adjacent tissue regions. Our previous study [1] investigated the presence of the different motion contributors and the modeling hereof, and resulted in 3 models describing the temporal and spatial varying contributions to the total motion from pulsation, breathing, and heart beat motion. The models were developed based on investigations of *in-vivo* RF-data. Simulations for the carotid artery were performed and evaluated.

This study addresses improvement of the models to achieve better simulated RF-data. Investigations of the ability to model and simulate tissue motion in the abdominal region are performed, and the results are presented. To explain the nature of vessel dilation a mathematical relation between the dilation and the pressure in the carotid artery is derived.

All simulations are based on the Field II program [2] using spatial impulse response and point scatterers. This program can handle any array transducer, focusing, apodization, and transducer excitation.

2 System and recording conditions

Modeling of the individual motions are based on investigation of *in-vivo* RF-data recorded at different positions revealing the motion information. The measurements was performed with a 3.2 MHz probe on a B&K 3535 ultrasound scanner connected

to a dedicated, real-time sampling system [3] capable of acquiring 0.27 seconds of data along one RF-line. The probe was hand-held, and data were obtained from 10 healthy volunteers. To cover the whole cardiac cycle each measurement was repeated 10 times, resulting in a data material consisting of 400 independent RF measurements of 950 pulse echo lines. No ECG synchronization could be performed, so it can not be guaranteed that the whole cardiac cycle was covered in the complete measurement set for each volunteer.

Dataset	Vessel	Scan plane	Motion
C1	Carotid artery	Transverse scan angle 90°	P,B
HV1	Hepatic vein	Right liver lobe intercostal scan	B,H (P)
HV2	Hepatic vein	Right liver lobe intercostal scan	H (P)
HV3	Hepatic vein	Left liver lobe epigastric scan	H (P)

Table 1: Recording conditions for determination of motion due to pulsation (P), heart (H) and breathing (B).

Table 1 lists the scan sites and the motions present during measurements. The subjects were lying supine. For the HV1 recordings the subjects were breathing shallowly to keep the vessel within the Doppler gate. During recordings of the HV2 and HV3 data, the subjects were told to hold their breath.

3 Models developed from *in-vivo* data

All models developed here and in [1] are based on investigation of the measured *in-vivo* RF-data. The data were bandpass filtered to remove noise, and the autocorrelator method [4] applied to obtain estimates of the tissue velocities. Thirty four adjacent RF-lines (temporally) were used to obtain high-quality estimates. Estimates of motion were obtained from the velocity estimates by summing over time at each depth. Plots of these estimates as a function of time and depth reveals the information needed to develop the motion models. In [1] the presence of motion in the surrounding tissue was found, and therefore it must be incorporated into the simulation to obtain realistic simulated data. All motion generators contribute to the total motion in the surrounding tissue. The individual contributors are assumed independent, so the accumulated tissue motion at a given scan-site can be computed by adding the contributions from the individual motions present. The tissue velocities are in the mm/s range with amplitude levels depending on scan-site, motions present, and distance between scanned region and the motion generators. Thereby the levels of tissue and blood motion at the vessel wall are in the same order, making it difficult to distinguish the signal components belonging to tissue and blood respectively.

Figures 1, 2, and 3 show examples of dilation plots, which visualizes features of the different motions over time and depth. The dilation is positive, if the scatterers move towards the transducer relative to an initial position, and negative if movement is away from the transducer.

3.1 Pulsation

The pulsation in the arteries is due to the time varying pressure in the vessel during a cardiac cycle, and results in a force acting on the vessel walls. A radial motion of the wall and the surrounding tissue [5] is induced. The pressure levels throughout a cardiac cycle in the carotid artery ranges from 80-160 mmHg. The relation between the dilation, d , and the pressure, p , can be approximated by a parabola [6, 7] as stated in Eq. 1, where p_0 is the diastole pressure and K a constant that accounts for the tissue characteristics. Equation 1 has been derived from excised arteries (mostly dog arteries), but is assumed to hold for *in-vivo* human arteries with proper choice of the tissue parameter K [8].

$$d = \sqrt{\frac{p(t) - p_0}{K}} = \sqrt{\frac{\Delta P}{K}} \quad (1)$$

In Fig. 1 dilation estimates due to pulsation in the carotid artery are visualized. Due to the radial nature of pulsation two dilation sequences moving in opposite directions relative to the center of the vessel occurs. The figure reveals the onset of a

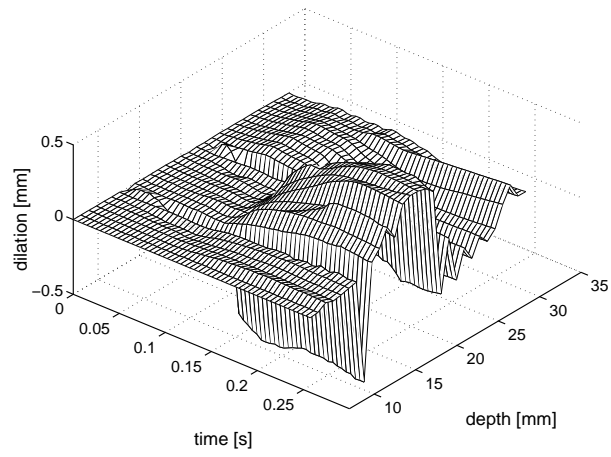


Figure 1: Example of dilation found from *in-vivo* data from the carotid artery. Pulse rate: 70 bpm.

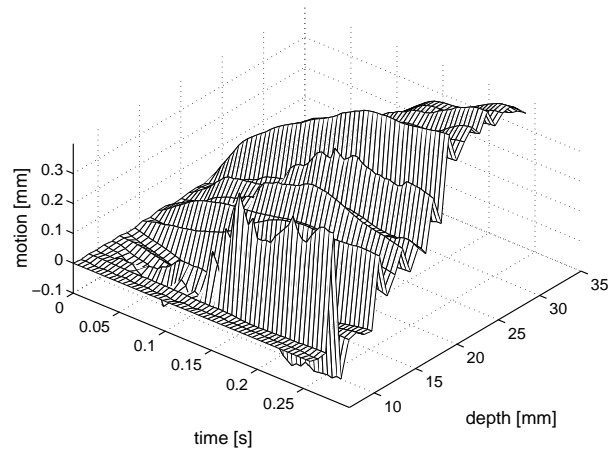


Figure 2: Example of breathing motion at carotid artery.

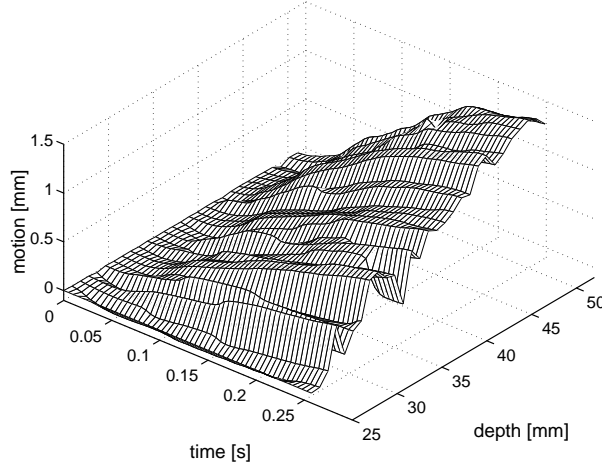


Figure 3: Example of motion due to heartbeat (HV3) at hepatic vein.

cardiac cycle and thereby dilation at time equal to 0.12 seconds. The preceding estimates reveals the dilation, when returning to diastolic conditions. The time sequence of the dilation rises fast and then decreases and returns to the initial value. All motion is relative to the center of the vessel, and the level of motion is damped with increased radial distance. The motion therefore is a function of time and depth, and assuming no correlation between time and depth the motion model becomes a product of two functions - one describing the time sequence, and the other describing the depth dependence. In Fig. 4(a) the temporal model for dilation due to pulsation for a given depth is shown with a pulse rate of 1 pulse/s. The temporal sequence agrees with the *in-vivo* dilation estimates obtained by Bonnefous [9].

In [1] the damping was modeled as a linear function of radius, which is not optimal. An exponential damping function, as given in Eq. 2, should be applied, where rd is the damping level at a given radius, r , b a constant, R_w the radius of the vessel, and R_l , the maximum radial distance at which motion will be seen. Beyond R_l the damping function is equal to zero.

$$rd = b(\cos(\pi \frac{r - R_w}{R_l - R_w}) + 1) \quad \text{for } R_w < r < R_l \quad (2)$$

3.2 Breathing

Figure 2 shows an example of motion due to breathing during inhalation. The lung "pushes" the tissue towards the transducer due to the location of the lung beneath the scan-site. The damping decreases with increasing depth. Again the motion is a function of time and space (as with pulsation). The repetition frequency will most often be lower, since the respiration frequency is lower than the heart beat frequency. The time sequence at a given depth is shown in Fig. 4(b). The model has a negative sign, since the motion is acting in the opposite direction of the positive axial axis (z -axis).

3.3 Heartbeat

Figure 3 shows an example of motion estimates due to the heart beating. It contains the same features as for breathing regarding position of motion generator, damping, and time sequence, but the repetition frequency is higher(- in average 1 beat/s). The contractions have been shown not to follow the same temporal sequence as pulsation, and is presumed to be due to the more complex motion pattern (translation as well as rotation) of the heart. The model for the tissue motion is given in Fig. 4(c), again assuming that the motion is acting in the axial direction.

All the models contain the same features regarding time and depth dependence, but the repetition time, amplitude, and damping vary with scan site and for the individual motion types. Additionally these model parameters vary among individuals.

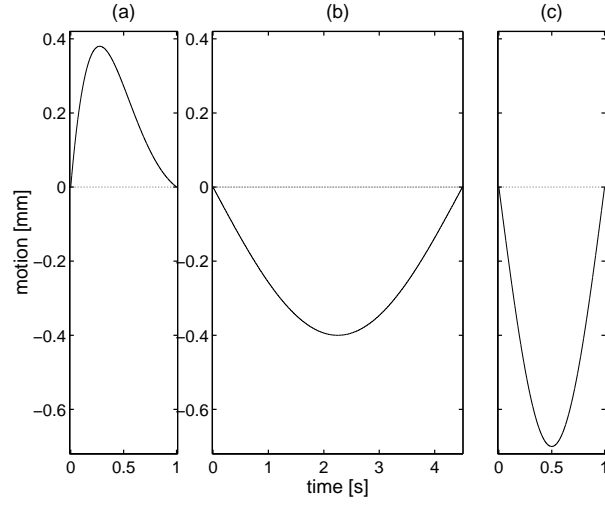


Figure 4: Models of dilation due to pulsation (a), breathing (b) and heartbeat (c). Frequency of breath: 13 breaths/min, pulsation and heartbeat: 60 pulses/min.

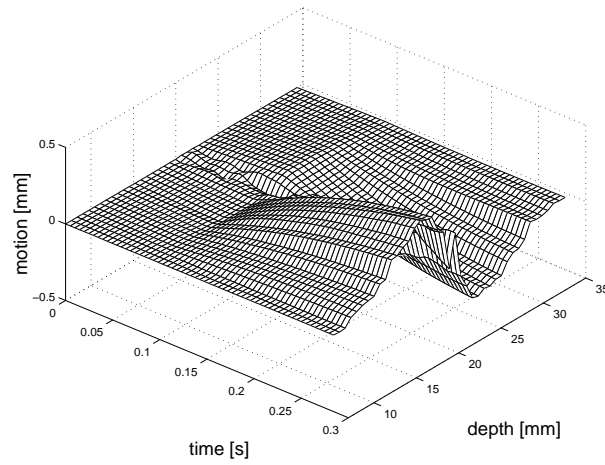


Figure 5: Estimates of dilation from simulated data mainly due to pulsation at the carotid artery. Pulse rate: 60 bpm.

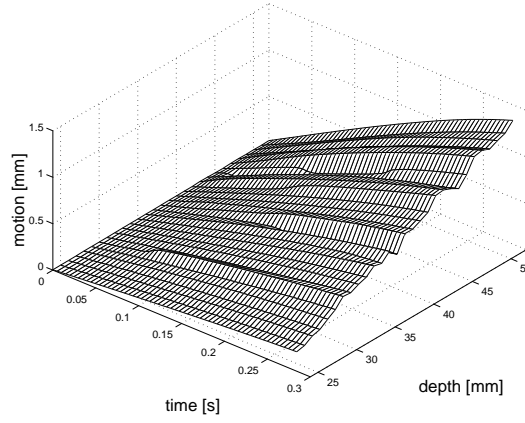


Figure 6: Motion estimates based on simulated data resembling the HV3 recordings (motion is due to the beating of the heart). Pulse rate: 60 bpm.

4 Simulations of motion

The ability to create realistic simulated data incorporating the motion has been verified for the carotid artery and the hepatic vein (HV3). The transducer was modeled as a 3.2 MHz convex, elevation focused array with 58 elements. A focusing and apodization scheme matching the used scan probe was incorporated. The point scatterers were given amplitude properties of tissue or blood, and moved around according to the motion model between each simulation of an RF-line. Womersley's pulsatile blood flow model [10] was used to determine the motion of the blood scatterers in the carotid artery. RF-data resembling 5 seconds was simulated to obtain data including the full effect from breathing and pulsation. Figure 5 shows an example of simulated dilation for the carotid artery. The damping was modeled by Eq. 2, with R_l equal to 20 mm. The scan angle was 90° . Comparing with Fig. 1 reveals a good agreement between the two dilations. The pulse rates differs for the two situations, giving a faster pulsation sequence for the higher pulse rate. In Fig. 1 some motion is present within the vessel (center of vessel at depth equal to 19 mm) - probably because the scan angle was not exactly 90° , so that the blood influences the motion estimates.

The blood flow in the hepatic can be modeled by a steady flow superimposed a time varying, low amplitude flow. In the HV3 simulations only the heart beat motion is present, requiring only 1 second of simulations to create RF-data covering a full cycle. The damping was modeled as a linear function of axial distance (z) with increasing amplitude for increased depth. The result of simulation is plotted in Fig. 6, and is to be compared with Fig. 3. The pulse rate for the real data is higher than for the simulated data, giving a faster motion sequence. Comparison reveals a good agreement between the motions, and simulation of realistic data for the abdominal region is thus possible.

5 Conclusion

The results presented here and in [1] proves presence of tissue motion. Motion models for each of the contributors have been developed and incorporated into the simulation program Field II. The generated simulated RF-data agrees well with *in-vivo* RF-data. Thereby a powerful tool for optimization of filters and estimators for processing of RF-signals have been obtained. The model parameters (amplitude, repetition frequency) vary depending on scan-site, motions present and the individual to be scanned. All of these can be modified in the program. A simple equation describing the relation between pressure and the dilation in the carotid artery has been derived, which explains the nature of the motion due to pulsation.

6 Acknowledgement

This project is supported by grant 9700883 and 9700563 from the Danish Science Foundation, grant 980018-311 from the Technical University of Denmark, and by B-K Medical A/S, Denmark. Paul Stetson is acknowledged for his assistance with

acquiring the *in-vivo* RF-data.

References

- [1] M Schlaikjer, S Torp-Pedersen, JA Jensen and PF Stetson, Tissue motion in blood velocity estimation and its simulation, Proc. 1998 IEEE Ultrasonics Symposium (1998) 1495.
- [2] JA Jensen, Users' guide for the Field II program, Technical report, Dept. of Info. Tech., Techn. Univ. Denmark (1998).
- [3] JA Jensen and J Mathorne, Sampling system for *in-vivo* ultrasound images, Medical Imaging V Symposium, SPIE 1444 (1991) 221.
- [4] C Kasai, K Namekawa, A Koyano and R Omoto, Real-time two-dimensional blood flow imaging using an autocorrelation technique, IEEE Trans. Son. Ultrason. 32 (1985) 458.
- [5] WW Nichols and MF O'Rourke, McDonald's Blood Flow in Arteries, theoretical, experimental and clinical principles, Lea & Febiger, Philadelphia (1990).
- [6] JD Bronzino, The Biomedical Engineering Handbook, CRC Press Boca Ranton, Boca (1995).
- [7] R Skalak and S Chien, Handbook of bioengineering, McGraw-Hill Book Company, New York (1987).
- [8] JO Arndt, J Klauske and F Mersch, The Diameter of the Intact Carotid Artery in Man and its change with Pulse Pressure, Plügers Archives 301 (1968) 230.
- [9] O Bonnefous, Stenoses dynamics with Ultrasonic Wall Motion Images, Proc. 1994 IEEE Ultrasonics Symposium (1994) 1709.
- [10] DH Evans, Some aspects of the relationship between instantaneous volumetric blood flow and continuous wave Doppler ultrasound recordings III, Ultrasound Med Biol 9 (1982b) 617.